WIS-78/49-ph

Inclusive Particle Spectra in $p(\pi^+)n$ Interactions at 195 Gev/c(*)

Y. Eisenberg, B. Haber, D. Hochman, U. Karshon, L. Lyons,†
E.E. Ronat, A. Shapira, R. Yaari and G. Yekutieli
Weizmann Institute of Science, Rehovot, Israel

ABSTRACT

We present results on single particle inclusive distributions in $p(\pi^+)n$ reactions from a Fermilab experiment using the hybrid 30" bubble-chamber and PWC facility. Distributions in rapidity (y), Feynman x and p_T^2 for π^+ and π^- are presented and compared with other experiments. The effects of different targets and projectiles (neutrons, protons and pions) on the distributions are demonstrated and discussed in terms of projectile and target fragmentation. The average transverse momentum $\langle P_T \rangle$ is studied as a function of x,y and multiplicity.

(*)Research supported by a grant from the United States-Israel Binational Science Foundation (BSF), Jerusalem, Israel.

† Permanent address: Nuclear Physics Laboratory, Oxford, England.

1. Introduction

Much progress has been achieved in the study of multiparticle production by hadrons at very high energies (>50 GeV) [1] since the CERN Intersecting Storage Rings (ISR) and the FNAL accelerator became available for experiments. At the ISR only pp interactions could be studied while the FNAL facility provided different beams ($\pi^\pm$,$K^\pm$,p) which were projected mainly on protons. A further development took place when the principal multiparticle detector at FNAL, the 30" bubble-chamber (BC), was supplemented by a system of Cerenkov counters and proportional wire-chambers (PWC)[2]. This increased the angular resolution and the accuracy of momentum measurements for tracks in the problematic forward cone. It also enabled to distinguish between different projectiles in the same exposure. Recently, exposures on deuterium have been carried out at FNAL enabling the study of multiparticle production on neutrons by different beams.

In this paper we report on pn and π^+n interactions studied with the hybrid BC-PWC system at FNAL. Some results from this experiment have been published previously [3-6]. Charged-particle multiplicities were presented [3] from a subsample of our scanned data. Revised values are given here. The neutron fragmentation region [4] and the production of slow protons [5] were studied using a subsample for which all tracks in the backward c.m. hemisphere have been measured. Finally, we have completed all the measurements including tracks in the forward c.m. hemisphere and adopted criteria to distinguish between protons and pions. The data presented in this paper are based on this entire sample. Some specific subjects like the inclusive π^+ to π^-

ratio and its relation to the quark model and an observation of mean-multiplicity hierarchies, which are also based on the entire sample, are published elsewhere [6].

The BC-PWC system and the experimental procedure are discussed in section 2. In section 3 we present the measured inclusive cross-sections and demonstrate the dependence of the inclusive reaction $a+b\to\pi^{\pm}+X$ (a denotes a proton or pion, b - proton or neutron) on: (1) the c.m. energy, (2) the nature of projectile and target, and (3) the charge of the pion. In section 4 we present and discuss the differences between the forward and backward c.m. hemispheres corresponding to the projectile and target fragmentation regions, respectively. In section 5 we present results on the dependence of average transverse momenta on various variables for various reactions. The results are summarized and conclusions are drawn in section 6.

2. Experimental Procedure

Our sample contains about 110,000 pictures from an exposure of the Fermilab 30-inch deuterium filled bubble chamber and proportional wire hybrid system to a mixed π^+ and p beam at 195 GeV/c. The experimental apparatus has been described elsewhere [2]. It consists of a Čerenkov counter and wire chambers upstream to the bubble chamber, which determine the beam identity and trajectory, and of several planes of downstream wire chambers, which give an improved momentum measurement of fast forward charged secondaries.

All the film was scanned twice, yielding a scanning efficiency of ∿98% for three or more outgoing charged particles. In order to obtain a pure sample of pn and π^+n interactions, we measured events with an odd number of prongs or an even number of prongs with a visible backward proton spectator in the laboratory system. Those events were

measured on the Spiral Reader automatic device and processed through the chain of programs POOH (filters and matches Spiral Reader data)-TVGP (reconstructs bubble chamber tracks in space)-PWGP (reconstructs wire chamber tracks)-TRACK ORGANIZER(matches bubble chamber with wire chamber reconstructed tracks). Tracks which failed to reconstruct properly were remeasured by a manual machine. All events were looked at on the scanning table and those tracks that still failed to reconstruct after a few measurements had their azimuth angle and momentum estimated with templates and a protractor. The dip angle for the "estimated" tracks was fixed at $(0\pm1)^{\circ}$, since almost all of them were fast non-dippy tracks. Our final sample includes 3275 pn events and 1371 π^+n events with three or more prongs in a predetermined fiducial volume.

In table 1 the efficiency of our measurement and processing procedure is summarized. The entries include all outgoing tracks in pn and π^+n interactions combined. 94.4% of the events are found to be complete (all prongs measured or estimated) and charged balanced - CCB (column 4). The difference between the number of expected and reconstructed tracks (columns 3 and 5) is due to incomplete events. The overall track efficiency (including estimated events) is 99%, but multiplicity dependent and falls from 99.6% for 3 prongs to 82.6% for 23 prongs. In order to remove fake tracks resulting from mismatches of POOH, we have looked at the distribution of the angle ψ in the plane transverse to the beam direction for all outgoing tracks. An isotropic distribution, as expected, is found in ψ for $p_T \leq 1.0$ GeV/c, where p_T is the transverse momentum. For tracks with higher p_T there is a concentration in the ψ distribution around 90°, probably due to mismatches. We have thus

excluded from our sample all tracks for which $72^{o} \leq \psi \leq 108^{o}$ and $p_T > 1$ GeV/c. The overall track efficiency after this cut drops to 97.6% (column 6, table 1), with a weak multiplicity dependence. About 3% of the outgoing tracks have a secondary interaction within less than 10 cm in space from the primary vertex. The effect of removing these tracks from our sample because of the large error on their momentum measurement, has been tested in various inclusive distributions and found to be insignificant. Similarly the exclusion of the "estimated" tracks (3.4% of the total) did not affect the various spectra, although the fraction of those tracks is multiplicity dependent (column 7). Thus short secondary tracks and "estimated" tracks were included in our final sample. The number of events with a visible backward spectator proton is also given in table 1 as a function of multiplicity. The fraction of these events ($\sim$18%) does not vary much with topology, indicating a good acceptance of short backward recoils up to the highest multiplicities.

Topological cross-sections $\sigma(n)$ for pn and $\pi^+ n$ interactions have been determined as explained in ref.3,(*) where several corrections were applied on the raw events before measurements, such as fiducial cuts and cuts on short secondary tracks. Due to these corrections and to the dependence of failure rates on topology, each event of multiplicity n has been multiplied for cross-section derivation by a weighting factor $\omega(n)=\sigma(n)/N(n)$, where $\sigma(n)$ is the corrected topological cross-section and N(n) is the number of successful events of the same multiplicity. It was shown previously [3] that in (14 ± 6)% of the events

(*)We use here updated cross-sections $\sigma(n)$ given in table 1 which differ slightly from our previously published results [3].

there is a double scattering (D.S.), i.e. one of the outgoing tracks scattered off the neutron, scatters again off the proton in the deuteron, yielding an even prong event which is not being measured. These lost events are biased towards high multiplicities and slow particles [7]. Our results were normalized to $\sigma(n)$ which included the D.S. correction as applied in [3], but we did not correct the detailed inclusive distributions, since such a procedure requires a specific detailed model which is not unique and is not expected to change the results significantly [6b].

Another possible source of bias comes from coherent events with an invisible deuteron in the final state, which are indistinguishable from neutron target events with an unobserved proton spectator. Those events are in general low-multiplicity diffractively excited events and are expected to contribute negligibly to the sample with five prongs and more, since at such multiplicities the deuteron will either break up or (due to t_{min} effects) be visible as a track recoiling in the forward direction, thus excluding the event from our sample. By assuming equal amounts of beam fragmentation (all charged particles emitted in the forward c.m. hemisphere) and of target fragmentation (one positive particle emitted in the forward c.m. hemisphere) in pn interactions, and assigning the difference to coherent deuteron events, we find a small fraction ($\sim$4%) of coherent events in the 3-prong sample and a negligible amount in the 5-prong sample, as expected. It is more difficult to estimate the coherent deuteron contamination for $\pi^+ n$ interactions, since the assumption of equal amounts of beam and target fragmentations is unjustified. Unless stated otherwise, no correction has been applied to the inclusive distributions in order to remove these events.

All negative particles are assumed to be π^-. No attempt has been

made to correct for K^- and $\bar{p}$, which have been estimated to contribute ~8% and 2% of the π^-'s respectively [8]. All K^+ (~10%, see [8]) are assumed to be π^+. Protons can be identified: (1) by ionization (slow protons, $p_{LAB}<1.4$ GeV/c); (2) when they are leading particles from an incoming proton (almost all particles with $x = 2P_L/\sqrt{s} > 0.6$, where P_L is the longitudinal momentum and $\sqrt{s}$ the total c.m. energy, are protons [8]). The inclusive charge exchange probability at the nucleon vertex has been determined [4] to be about 0.4. Thus we expect, on the average, about 0.4 protons at the neutron vertex and ~0.6 protons at the proton vertex and altogether one proton per event for pn interactions. For the pn sample a leading particle ($x > 0.6$) was found in 24% of the events and a slow proton in 19%. Thus, about 43% of the protons could be identified, leaving an average of 0.57 unidentified protons per event. The average number of positive particles for the pn sample is 4.28 ± 0.04 (see table 3) and of these 3.85 do not contain an identified proton. Thus, the "π^+-sample" would contain a 15% contamination due to misidentified protons. To reduce this contamination we have adopted the following procedure:

(a) Forward CM hemisphere. For the pn data positive tracks with $x > 0.6$ were taken as protons. For the rest of the events we have randomly chosen a fraction of the events in which the fastest positive particle, when assumed to be a proton, is emitted in the forward hemisphere such that by assigning a proton mass to these tracks the overall proton yield in the forward hemisphere is consistent with the required 60%. All other positive tracks were assumed to be pions. For the π^+n data all positive particles emitted in the forward hemisphere were assumed to be pions.

(b) Backward hemisphere. pn and π^+n interactions have been treated in the same way. For events without a slow identified proton the positive

track with smallest rapidity emitted in the backward hemisphere and unidentifiable by ionization ($p_{LAB}>1.4$ GeV/c) was assumed to be a proton. By this procedure we obtained a proton yield of 35% (38%) for pn (π^+n) interactions close to the expected yield of 40% mentioned above. All the data in this paper have been corrected as described above, unless specified otherwise.

Monte-Carlo calculations have been performed in order to check the reliability of the corrected p sample in the backward hemisphere. In these calculations we assumed a typical neutron fragmentation to $N^* \to p\pi^-\pi^0$ with mass M=1.6 GeV, width Γ = 200 MeV, production matrix element exp.[8t] and isotropic decay distribution. In figure 1, the experimental rapidity (y_{CM}) and transverse momentum (p_T) distributions of the corrected backward protons produced in the pn sample are compared with the Monte-Carlo spectra, normalized to the data. The agreement for such a crude model is reasonable.

There is some uncertainty in the value of the variables considered in this experiment due to the Fermi motion of the neutron target in the deuteron. For events with a visible backward spectator, the neutron target four-momentum is known and given by the difference of the deuteron and proton spectator four momenta. For events with an invisible spectator, the three-momentum of the neutron was taken as $p_x=p_y=p_z=0$ in the laboratory system, and its energy was calculated from the average value of the square of the three-momentum (0.0035 $(GeV/c)^2$), assuming a Hulthen distribution for the Fermi motion of the neutron. The uncertainty in the variables due to the Fermi motion is usually smaller than the bin width of the distributions. However, this effect occasionally results in the momentum of an outgoing particle exceeding its physical limit, in addition to the more severe smearing

caused by poor momentum resolution from the track measurement. The momentum of these particles was reassigned to a fixed value at the physical limit.

Throughout this paper the multiplicity of events refers to interactions on a neutron target, and thus a visible backward spectator proton is not counted and no even prong events are mentioned in the discussion of the data.

3. Inclusive $\pi^{\pm}$ production

Figures 2 to 6 show the measured cross-sections and demonstrate the dependence of the inclusive reaction $a+b \to \pi^{\pm}+X$ on: (a) the charge of the produced pion, (b) the c.m. energy and (c) the nature of the target and projectile. In figures 2 and 3 we present the measured inclusive cross-sections for $pn \to \pi^{\pm}X$ and $\pi^+n \to \pi^{\pm}X$ at 195 GeV/c in terms of the c.m. rapidity y_{CM} and the Feynmann variable $x(=\frac{2p_L}{\sqrt{s}})$. All negative particles were considered to be pions and positive pions were defined as explained in the previous section. For both reactions the π^- cross-sections exceed those of the π^+ in the backward c.m. hemisphere while in the forward hemisphere the π^+ cross-sections exceed those of the π^-. From fig.2 we also notice that the excess of π^+ over π^- in the forward hemisphere is larger for π^+n than for the pn reaction. These observations can be explained in terms of neutron, proton and pion fragmentation. When a neutron fragments at least one baryon is produced and the number of negative particles is equal to the number of positive ones. Let α be the probability of the baryon to be a proton, then the average number of π^- will exceed the number of π^+ by α if

strange particles and antibaryon production are neglected. Similarly, since the proton can fragment into neutron + pions we shall expect more π^+ than π^- in p fragmentation (a difference of α by charge invariance). For π^+ fragmentation the difference will be 1.0. Thus, since the neutron fragmentation is predominantly in the backward hemisphere and proton or π^+ fragmentations in the forward hemisphere, one should expect more π^- for $y_{CM}<0$ and more π^+ for $y_{CM}>0$. Furthermore, the π^+ excess in the forward hemisphere is expected to be larger for π^+ reactions than for p reactions in agreement with our observations.

In figure 4 we have plotted the inclusive $pn \to \pi^-X$ cross-section at 195 GeV/c together with the cross-section for $pn \to \pi^-X$ at 11.6 GeV/c [9]. Note that $\frac{d\sigma}{dy_{LAB}}$ scales for $y_{LAB}<0.8$ (neutron fragmentation region) over the large energy range considered. For higher rapidities $\frac{d\sigma}{dy_{LAB}}$ increases with c.m. energy. Similar observations have also been made for pp reactions [8].

In figure 5 we compare the reactions $pn \to \pi^{\pm}X$ and $\pi^+n \to \pi^{\pm}X$ (same target) at 195 GeV/c. Because of the large difference in σ_{inel} for the two reactions we use the normalized cross-sections $\frac{1}{\sigma_{inel}} \frac{d\sigma}{dy_{CM}}$. For π^- production the normalized cross-sections coincide in the neutron fragmentation region ($y_{CM} < -2.0$) and agree, within errors, over the whole backward hemisphere. Large and significant deviations are observed in the forward hemisphere in particular for higher y_{CM} (proton or π^+ fragmentation regions). A similar behaviour is observed for π^+ production: the cross-sections coincide, within errors, in the backward hemisphere and strongly deviate in the forward hemisphere.

In figure 6 we compare the inclusive cross-sections for $pn \to \pi^-X$ at 195 GeV/c with those for $pp \to \pi^-X$ at 205 GeV/c [8]. The comparison is

between reactions with the same projectile and different targets at a similar energy. Since $\sigma_{inel}(pp) \approx \sigma_{inel}(pn)$ the measured cross-sections can be directly compared. A clear and significant excess of negative pions is observed for the pn data in the backward hemisphere (different target) while in the forward hemisphere (same projectile) the cross-sections seem to overlap. The difference in cross-sections for $y_{CM}>2.0$ may be attributed (at least partly) to the difficulties in momentum resolution and different treatment of very high-energy particles in the two experiments.

From figs. 5 and 6 we conclude that $\pi^{\pm}$ production in the various hemispheres is closely connected with the nature of the particles fragmented in the hemisphere. Similar cross-sections are obtained for hemispheres containing the same particle although the reactions are different. This confirms the validity of fragmentation and factorization arguments for high energy NN and πN reactions.

The π^+ and π^- inclusive distributions in the transverse momentum squared, p_T^2, are shown in fig.7 for both pn and π^+n reactions. For comparison we have also plotted in fig.7a the $pn \to \pi^- X$ distribution at 11.6 GeV/c [9] and the $pp \to \pi^- X$ distribution at 205 GeV/c [8]. The latter (solid line) is the distribution fitted to the form $Ae^{-Bp_T^2} + Ce^{-Dp_T^2}$ as given in ref.[8]. The various distributions (at ≈200 GeV/c) are roughly similar in shape. Differences in magnitude are due to overall cross-section differences for the specific reactions. Fits to an exponential function $Ae^{-Bp_T^2}$ over the whole p_T^2 range yield high χ^2 values. The distributions were therefore fitted to a sum of two exponentials: $Ae^{-Bp_T^2} + Ce^{-Dp_T^2}$. The results of the fits are given in table 2 together with the $pp \to \pi^- X$ results at 205 GeV/c and the $pn \to \pi^- X$ results at 11.6 GeV/c.

From table 2 we conclude that the overall p_T^2 distributions can be reasonably fitted ($P(\chi^2)>2\%$) for all reactions by a sum of two exponentials in the range $0.0 \leq p_T^2 \leq 0.7$ $(GeV/c)^2$. We find that both slopes B and D are equal within error for all neutron reactions at ≈200 GeV/c (B≈0.0 and D≈4.5 $(GeV/c)^{-2}$). B increases with energy from 11.6 to 195 GeV/c while D does not change very much. The two slopes are higher for neutron reactions than for pp reactions.

In fig. 8 we show the $\pi^{\pm}$ inclusive distributions in rapidity for three multiplicity groups: (a) for 3-5 prongs, (b) for 7-9 prongs, and (c) for more than 9 prongs. In pn reactions, $\frac{d\sigma}{dy_{CM}}$ for the 3-5 prong group is "flatter" than for higher multiplicities. A similar behaviour is observed in pp reactions [8]. For π^+n reactions some structure is observed in the 3-5 prong distribution while the shape of the higher multiplicities is similar to those for pn reactions.

Finally we present the measured ratio of π^+ to π^- as a function of rapidity for both pn and π^+n reactions. From isospin invariance (and also from quark model arguments [10]) we would expect that the π^+/π^- ratio R from proton fragmentation should be equal to the π^-/π^+ ratio 1/R from neutron fragmentation. We have therefore plotted the ratio R', defined as $R'=R$ for $y_{CM}>0.0$ and $R'=\frac{1}{R}$ for $y_{CM}<0.0$, versus the c.m. rapidity in Fig.9. From Fig.9 we observe that: (a) R' increases with $|y_{CM}|$ for both reactions. (b) R' is symmetric (within errors) about $y_{CM}=0$ for the pn reaction ($R'(y)=R'(-y)$).(c) The R' values for pn and π^+n reactions are equal, within errors, in the backward hemisphere while they are different in the forward hemisphere. The R' dependence on other kinematical variables (x_R, p_T etc..) and its relation to quark-model predictions are discussed elsewhere [6a].

4. The Negative Excess and Forward-Backward Comparison

The most outstanding difference between inclusive pn and pp reactions is the y-distribution of the charged secondaries (see e.g. fig.6). In table 3 we present an updated summary of the average number of negative, positive and charged particles, in both c.m. hemispheres, for the reactions pn and π^+n at 195 GeV/c. For comparison we also cite the results for the pp reaction at 205 GeV/c [8] and for π^+p at 200 GeV/c [11]. We first consider the overall charged multiplicities which are nearly equal for pn and pp reactions. The small difference $\Delta^c \equiv \langle n_c \rangle_{pn} - \langle n_c \rangle_{pp} = -0.12 \pm 0.09$ is related [4] to the charge exchange α at the nucleon vertex (already discussed above). We find $\alpha = \frac{1}{2}(1+\Delta^c) = 0.44 \pm 0.04$ in good agreement with previous measurements [12]. The backward-forward asymmetry ($\Delta_2^c = \langle n_c \rangle^B_{pn} - \langle n_c \rangle^F_{pn} = -0.12 \pm 0.05$) can also be related to α as discussed below. However a part of this difference may also be attributed to kinematic effects caused by misidentification of particles. (If a particle is misidentified to have a smaller mass (e.g. a kaon as a pion) the experimental procedure will tend to increase its rapidity and therefore increase the "observed" particles in the forward hemisphere).

Unlike pp reactions where backward-forward (B-F) symmetry is anticipated, we find strong B-F asymmetries for both $\langle n- \rangle$ and $\langle n+ \rangle$ in pn reactions. These effects are presumably due to the different fragmentation of the proton and neutron into positive or negative particles. Since the study of positive particles is complicated by the π^+-K^+-p ambiguities we shall concentrate on the negative particles where the contamination of K^- and antiprotons is $\leq 10\%$. Thus $\Delta_1^- \equiv \langle n_- \rangle^B_{pn} - \langle n_- \rangle^B_{pp} = 0.37 \pm 0.03$ can be used as an estimate of the excess of negative particles

from neutron fragmentation over those from proton fragmentation(*). Another estimate of this negative excess is given by $\Delta_2^- \equiv \langle n_- \rangle^B_{pn} - \langle n_- \rangle^F_{pn} = 0.30 \pm 0.03$ where the comparison is between the backward neutron and the forward proton in the same experiment. A rough estimate(*) shows that we should expect $\Delta_1^- = \Delta_2^-$ if all the fragmented particles stay in the c.m. hemisphere of the original nucleon and that $\Delta_1^- > \Delta_2^-$ if there is some particle transfer through the $y_{CM}=0$ boundary into the other c.m. hemisphere. Thus the value of $\Delta_1^- - \Delta_2^- = 0.07 \pm 0.03$ may indicate that the negative charge transfer from the neutron hemisphere to the proton is larger than the reverse.

The rapidity distribution of the negative excess is shown in fig. 10 where the difference in cross-sections $\delta_1(y) = \frac{d\sigma(pn\to\pi^- X)}{dy} - \frac{d\sigma(pp\to\pi^- X)}{dy}$ between pn and pp in the backward hemisphere is plotted. On the same figure we also plot $\delta_2(y) = \frac{d\sigma(y)}{dy} - \frac{d\sigma(-y)}{dy}$, i.e. the backward minus

(*)Consider a crude model in which the particles produced in pn reactions come from three sources: proton fragmentation, neutron fragmentation and some other source (central region). Let $\alpha, (b_1+b_2)$ and (c_1+c_2) denote the average number of protons, positive ($\pi^+, K^+ \cdots$but non-proton) and negative (π^-, K^-) particles, respectively produced in neutron fragmentation. b_1 is the number of positives in the c.m. hemisphere of the original neutron and b_2 are those found in the other hemisphere, etc. Then, by isospin invariance, the number of protons, positive and negative particles from proton fragmentation will be $(1-\alpha)$, (c_1+c_2), (b_1+b_2) respectively (antiprotons and other baryons are neglected). If the third source is the same for pp and pn reactions and is symmetric about $y_{CM}=0$ the following relations are easily derived:

$$\Delta_1^- \equiv \langle n_- \rangle^B_{pn} - \langle n_- \rangle^B_{pp} = c_1 - b_1 \qquad \Delta_1^c \equiv \langle n_c \rangle^B_{pn} - \langle n_c \rangle^B_{pp} = 2\alpha - 1$$

$$\Delta_2^- \equiv \langle n_- \rangle^B_{pn} \langle n_- \rangle^F_{pn} = (c_1 - b_1) - (c_2 - b_2) \qquad \Delta_2^c \equiv \langle n_c \rangle^B_{pn} - \langle n_c \rangle^F_{pn} = 2\alpha - 1$$

Experimentally, we find $\Delta_1^c = -0.12 \pm 0.05$, $\Delta_2^c = -0.12 \pm 0.04$ from which we deduce the value $\alpha = 0.44$. We also find that $\Delta_1^- - \Delta_2^- = (c_2 - b_2) = 0.07 \pm 0.03$.

forward cross-sections for $pn \to \pi^-$ as a function of $y(\equiv y_{CM})$. The two distributions have a similar shape and in general $\delta_1(y) > \delta_2(y)$. The similarity in shape supports our interpretation that both $\delta_1(y)$ and $\delta_2(y)$ measure the same negative excess as discussed above.

To check the negative excess for various multiplicities we have divided our samples into three groups: a) events with 1-2 negative pions, b) with 3-4 negative pions and c) more than 4 negative pions. For each group we have plotted in fig.11 the normalized inclusive π^- cross-section $\frac{1}{\sigma(N)} \cdot \frac{d\sigma^-(N)}{dy_{CM}}$ for both pn and pp reactions. $\sigma(N)$ is the inelastic cross-sections for N pi minuses, $\frac{d\sigma^-(N)}{dy_{CM}}$ is the inclusive π^- distribution and N = 1,2 for the first groups, N = 3,4 for the second, etc. A clear negative excess is seen for all three multiplicity groups consistent with the fragmentation picture as discussed above. This shows that the negative excess occurs in all n's and thus is not due only to the diffractive component.

For the π^+ reactions we find from table 3 that $\langle n_c \rangle_{\pi^+ n} - \langle n_c \rangle_{pn} = 0.21 \pm 0.11$ and $\langle n_c \rangle_{\pi^+ p} - \langle n_c \rangle_{pp} = 0.22 \pm 0.24$. This shows that the number of charged particles produced in π^+ reactions exceeds those from p reactions (on the same target) by about 0.2 at 200 GeV/c. The same excess is found for both proton and neutron targets. For π^+ reactions we also find $\langle n_c \rangle_{\pi^+ n} - \langle n_c \rangle_{\pi^+ p} = -0.13 \pm 0.24$ yielding (as expected) the same charge-exchange value at the neutron vertex ($\alpha = 0.44$) as derived above from proton reactions. Unlike pn reactions a large forward-backward asymmetry for charged particles ($\langle n_c \rangle^F_{\pi^+ n} - \langle n_c \rangle^B_{\pi^+ n} = 0.67 \pm 0.07$) and practically no asymmetry for negative particles ($\langle n_- \rangle^F_{\pi^+ n} - \langle n_- \rangle^B_{\pi^+ n} = 0.04 \pm 0.04$) are found for $\pi^+ n$ reactions. These differences are probably related to the different fragmentation of the π^+ and the proton but

are too complicated for a quantitative explanation(*).

In fig.12 we present $N_{Backward}/N_{Total}$, for negative and positive secondaries, as a function of multiplicity. For pn reactions $\frac{N_B}{N_T} \to 0.5$ as n increases (negative particles from above, positive from below) and $\frac{N_B}{N_T} \approx 0.5$ for $n \geq 13$. The positive value of $(\frac{N_B}{N_T} - 0.5 = \frac{2 \cdot N_B - N_T}{2 \cdot N_T})$ for negative particles can be explained by the excess of negatives in neutron fragmentation over those in proton fragmentation. The negative value of $(\frac{2 \cdot N_B - N_T}{2 \cdot N_T})$ for positive particles is related to the value $\alpha \approx 0.4$ which will yield more protons from proton fragmentation than from neutron fragmentation. In both cases $(2 \cdot N_B - N_T)$ is not expected to change much with multiplicity while the demoninator $2 \cdot N_T$ increases with multiplicity. We, therefore, would expect $|\frac{2 \cdot N_B - N_T}{2 \cdot N_T}|$ to decrease with multiplicity in agreement with our observations.

Note that the ratio N_B/N_T is underestimated if our sample contains an appreciable fraction of coherent deuteron events. In this case the charged particles will appear in the forward hemisphere and N_B/N_T will be underestimated. We have shown in section 2 that the coherent deuteron contamination can be neglected for $n \geq 5$. For n=3 a small correction (~ 0.02) in N_B/N_T is estimated for the pn reaction. The correction for $\pi^+ n$ reaction (and n=3) may be considerably larger.

(*) In terms of the model mentioned above there is no obvious reason to assume a symmetric F-B contribution from the third source (central region) for $\pi^+ n$ reactions while it is reasonable for nucleon-nucleon reactions. Thus part of the asymmetry in $\pi^+ n$ reactions may be related with the central region and not only with fragmentation. If, however, we attribute the difference between any two reactions a+b→anything and a'+b→anything only to the difference in a and a' fragmentation and assume the same central region contribution for both reactions then, an interesting hierarchy for the fragmentation of various particles into charged objects emerges. This possibility is discussed in detail in ref. 6b and references therein.

For π^+n reactions, the backward excess of negatives due to neutron fragmentation will be compensated by the increase in negatives from the pion fragmentation in the forward hemisphere (we have seen above that the number of charged particles from π fragmentation is higher than from nucleon fragmentation). This may yield a constant value of $\frac{N_B}{N_T} = 0.5$ for all multiplicities. A higher π than proton fragmentation would imply that $\frac{N_B}{N_T}$ for π^+n should be smaller than for pn in agreement with the observation.

The overall charge multiplicities at 200 GeV/c can be compared with those at 100 GeV/c. Using the results and compilation of Lys et al. [13] we find at 100 GeV/c $\langle n_c\rangle_{pn}-\langle n_c\rangle_{pp} = -0.19 \pm 0.12$ and $\langle n_c\rangle_{\pi^+n}-\langle n_c\rangle_{\pi^+p} = -0.24 \pm 0.16$ yielding $\alpha = 0.41 \pm 0.06$ and $\alpha = 0.38 \pm 0.08$ respectively in agreement with our result at 200 GeV/c. Similarly we find at 100 GeV/c $\langle n_c\rangle_{\pi^+n}-\langle n_c\rangle_{pn} = 0.37 \pm 0.17$ and $\langle n_c\rangle_{\pi^+p}-\langle n_c\rangle_{pp} = 0.32 \pm 0.10$ compared to 0.21 ± 0.11 and 0.22 ± 0.24 at 200 GeV/c. If the last differences are real (and not due to statistical fluctuations or systematic effects due to the use of different experiments) then it agrees with the prediction of Pajares et al.[14] on the decrease of $\langle n_c\rangle_{\pi^+p}-\langle n_c\rangle_{pp}$ with energy and indicates that such a decrease would also occur for $\langle n_c\rangle_{\pi^+n}-\langle n_c\rangle_{pn}$.

5. $\langle p_T\rangle$ - Average of Transverse Momenta

In table 4 we present average transverse-momenta $\langle p_T\rangle$, in the backward ($\langle p_T^{\pm}\rangle_B$) and forward ($\langle p_T^{\pm}\rangle_F$) c.m. hemispheres for the reactions $pn\to\pi^{\pm}X$ and $\pi^+n\to\pi^{\pm}X$ at 195 GeV/c. For comparison we also present $\langle p_T\rangle$ values for the reactions $pp\to\pi^-X$ at 205 GeV/c [8] and $pn\to\pi^-X$ at 11.6 GeV/c. The following conclusions can be drawn from table 4:

(a) the same $\langle p_T^-\rangle_B$ (=0.336 GeV/c) is obtained for reactions (1),(3) and (7) (inclusive π^- production at 200 GeV/c). This value is significantly higher than for $pn\to\pi^-X$ at 11.6 GeV/c. (b) $\langle p_T^-\rangle_F$ for $pn\to\pi^-X$ and $\pi^+n\to\pi^-X$ are somewhat higher than $\langle p_T^-\rangle_B$ for the same reactions but still consistent with it. (c) $\langle p_T^+\rangle_B$ for $pn\to\pi^+X$ and $\pi^+n\to\pi^+X$ are consistent with $\langle p_T^-\rangle_B$ for $pn\to\pi^-X$ and $\pi^+n\to\pi^-X$. This is, however, not true for pp where $\langle p_T^+\rangle_B > \langle p_T^-\rangle_B$. (d) $\langle p_T^+\rangle_F > \langle p_T^+\rangle_B$ for pn and to a greater extent for π^+n reactions.

For the pn reactions one would expect, from isospin invariance, that $\langle p_T^+\rangle_B = \langle p_T^-\rangle_F$ and $\langle p_T^+\rangle_F = \langle p_T^-\rangle_B$. The second relation is obviously violated but part of the $\langle p_T^+\rangle_F - \langle p_F^-\rangle_B$ difference ($\sim$0,010) can be attributed to a small proton contamination in the forward π^+ sample, Such a contamination would yield a higher $\langle p_T^+\rangle$ since the $\langle p_T\rangle$ for protons is larger than for pions [15]. The correction for this effect will reduce the $\langle p_T^+\rangle_F - \langle p_T^-\rangle_B$ difference to about 0.010-0.015 which is not inconsistent with zero within statistical errors but may also be of a systematic origin. For the π^+n reactions $\langle p_T^-\rangle_B$, $\langle p_T^-\rangle_F$ and $\langle p_T^+\rangle_B$ are equal within errors (or within the $\sim$0.010 level) while $\langle p_T^+\rangle_F$ is significantly larger. This difference is related with the high $\langle p_T^+\rangle_F$ found for low-multiplicity and/or high x events as will be shown below. The difference $\langle p_T^+\rangle_B - \langle p_T^-\rangle_B$ for pp reactions at 205 GeV/c (ref.8) can also be explained, in part, by a proton contamination in the pion sample as discussed above. Finally, we have also added in table 4 the $\langle p_T\rangle$ values for protons in pn and π^+n reactions (in brackets). The errors are statistical only and large systematic deviations are possible since most of the protons were not identified by ionization but were selected by the procedure discussed in section 2. However, the high values of

$\langle p_T \rangle$ and the fact that the three $\langle p_T \rangle$ values are equal within errors show that our mass-assignment procedures are reasonable.

In figs.13 to 15 we show the $\langle p_T \rangle$ distributions for the reactions $pn \to \pi^{\pm} X$ and $\pi^+ n \to \pi^{\pm} X$ as functions of x, $x_R (= \frac{2p}{\sqrt{s}})$, y_{CM} and the multiplicity n, where p is the absolute momentum of the $\pi^{\pm}$ in the center of mass system. Due to the low statistics for the regions $|x|$ and x_R above 0.5 the results in fig.13 are plotted for $|x|, x_R < 0.5$ only except for $\pi^+ n \to \pi^+ X$ where $\langle p_T \rangle$ is given up to x=1.0 in the inset of fig.13b. Errors are statistical and plotted at selected points. Dips are seen around x=0 (seagull effect) and x_R=0. The latter is more pornounced as expected from kinematical considerations. However, no depletion is seen in the $d\langle p_T \rangle / dy$ distributions around y=0 (figs. 14a and 14b).

In figs. 14c, 14d and 15 we present the $\langle p_T \rangle$ distribution vs. the multiplicity n. For n>3 $\langle p_T \rangle$ tends to decrease with multiplicity (fig.14c,14d) in particular for $n \geq 9$. A similar effect has also been observed in pp interactions [8]. We also note that high $\langle p_T^+ \rangle$-s are found for forward π^+ in the $\pi^+ n$ reaction for: (1) high x values (fig.13b inset) and (2) low multiplicity (fig.15d). Further investigation shows that the two classes are correlated and that they contribute to the high $\langle p_T^+ \rangle$ value for $\pi^+ n$ in the forward hemisphere (table 4).

6. Summary and Conclusions

We conclude with a short summary of our main results and their interpretation. In general, many features of the data can be explained in terms of projectile and target fragmentation. Our pn and $\pi^+ n$ events obtained in the same experiment, provide an unbiased sample from which

the fragmentation of protons, positive pions and neutrons can be studied. From this sample and by comparison with pp interactions at 205 GeV/c [8] and pn interactions at 11.6 GeV/c we get the following results:

(1) At the same c.m: energy (∿200 GeV/c) pion inclusive cross-sections for various reactions are similar for c.m. hemispheres which contain the same fragmented particle (projectile or target). Explicit examples are $\pi^{\pm}$ distributions in the backward hemispheres of pn and $\pi^+ n$ (neutron fragmentation, fig.5) or in forward pn compared to pp reactions (proton fragmentation, fig.6).

(2) There is an excess of negative pions in the neutron hemispheres over the proton hemispheres. It persists for various multiplicities (fig.11) and the same negative excess is found by comparing forward vs. backward pn hemispheres or from pn vs. pp backward hemispheres (fig.10). This excess is anticipated since π^- can be produced already in two-body neutron fragmentation ($p\pi^-$) while only in three-body (and more) proton fragmentation.

(3) The equality of $\langle n_c \rangle_{pn} - \langle n_c \rangle_{pp} = \langle n_c^B \rangle_{pn} - \langle n_c^B \rangle_{pp} = \langle n_c^B \rangle_{pn} - \langle n_c^F \rangle_{pn} = -0.12$ implies a value of $\alpha = 0.44 \pm 0.04$ for the fragmentation of a neutron into a proton (or a proton into a neutron). This value is somewhat higher but consistent with that found for lower energies [12].

(4) $d\sigma(pn \to \pi^- X)/dy_{LAB}$ scales for $y_{LAB} < 0.8$ (neutron fragmentation region) over the energy range 11.6-195 GeV/c (fig.4).

(5) $\frac{d\sigma}{dp_T^2}$ for pn and $\pi^+ n$ interactions cannot be parametrized by a single exponential but yields reasonable fits to $Ae^{-Bp_T^2} + Ce^{-Dp_T^2}$. The slopes B and D are equal within errors for all neutron reactions and are higher than for pp reactions. B increases with energy between 11.6 and 195 GeV/c.

(6) Dips in $\langle p_T \rangle$ around x=0 (seagull effect) and x_R=0 are found for pn and $\pi^+ n$ reactions but no depletion is seen in $\langle p_T \rangle$ vs. y_{CM} at y_{CM}=0.
(7) Similar $\langle p_T \rangle$ values are found in the backward hemisphere for pn and $\pi^+ n$ reactions ($\sim$0.335 GeV/c). However, high $\langle p_T^+ \rangle$ values are found for $\pi^+ n \to \pi^+ X$ in the forward hemisphere. Most of this difference is due to low-multiplicity and/or high-x events.

Acknowledgments

We wish to acknowledge the diligent and excellent work of our scanning, programming and electronics teams. We are grateful to the Fermilab staff and the PHS Consortium for making this experiment possible. The early stages of this experiment were performed in collaboration with the Strasbourg Hydrogen Bubble-Chamber group.

References

1. See e.g. J. Whitmore, Phys. Rep. 27C (1976) 187.
2. D.G. Fong et al., Phys. Lett. 53B (1974) 290; Nucl. Phys. B102 (1976) 386.
3. Y. Eisenberg et al., Phys. Lett. 60B (1976) 305.
4. Y. Eisenberg et al., Phys. Lev. Lett. 38 (1977) 108.
5. Y. Eisenberg et al., Nuc. Phys. B135 (1978) 189.
6. (a) Y. Eisenberg et al., "Inclusive π^+ to π^- ratios in $\pi^+ n$ and pn interactions at 195 GeV/c", WIS - 78/19-Ph (preprint).
   (b) Y. Eisenberg et al., "Hierarchy of mean multiplicities in pn and $\pi^+ n$ interactions at 195 GeV/c", Phys. Lett. B, in press (1979).
7. W. Busza et al., Phys. Rev. Lett. 34 (1975) 836; W. Busza, Acta Phys. Pol. B8 (1977) 333; C. Halliwell et al., Phys. Rev. Lett. 39 (1977) 1499.
8. T. Kafka et al., Phys. Rev. D16 (1977) 1261.
9. D. Hochman et al., Nucl. Phys. B89 (1975) 383.
10. R.D. Field and R.P. Feynman, Phys. Rev. D15 (1977) 2590; Nucl. Phys. B136 (1978) 1.
11. J. Erwin et al., University of California, Davis, Rep. No. UCD-PRL-9-15-75 (1975).
12. U. Idschok et al., Nucl. Phys. B67 (1973) 93.
13. J.E.A. Lys et al., Phys. Rev. D16 (1977) 3127.
14. C. Pajares and R. Pascual, "Analysis of πp and pp Multiplicities", TH-2375-CERN Preprint Aug. 1977.
15. See e.g. A. Bigi et al., Proc. 1962 Int. Conf. on High-Energy Physics at CERN (1962).

Table 1: Event and track statistics for pn and π^+n interactions (combined). Revised multiplicity cross sections are given in the last two columns. The prong count refers to interactions on a neutron target and visible spectator protons are not counted.

No. of prongs	No. of events	Expected no. of tracks	No. of CCB events	No. of tracks found	No. of tracks used	% of estimated tracks	No. of visible backward spectators	σ_{pn}(mb)[a]	σ_{π^+n}(mb)[a]
3	860	2580	845	2570	2555	1.3	177	5.19 ± 0.19	3.00 ± 0.18
5	1008	5040	984	5021	4972	1.4	186	5.72 ± 0.20	3.50 ± 0.20
7	978	6846	937	6809	6718	1.5	170	5.73 ± 0.20	4.13 ± 0.22
9	761	6849	708	6781	6676	2.6	134	5.31 ± 0.19	3.21 ± 0.19
11	552	6072	504	6016	5893	3.7	92	3.60 ± 0.16	2.60 ± 0.17
13	315	4095	284	4031	3972	5.8	62	2.67 ± 0.14	1.66 ± 0.14
15	98	1470	78	1432	1409	8.7	14	1.34 ± 0.10	0.77 ± 0.09
17	54	918	46	902	884	11.8	8	0.63 ± 0.07	0.58 ± 0.08
19	15	285	8	253	252	25.0	3	0.12 ± 0.03	0.10 ± 0.03
21	4	84	1	74	74	31.1	2	0.05 ± 0.02	0.08 ± 0.03
23	1	23	1	19	19	26.3	0	0.01 ± 0.01	0.01 ± 0.01
Total	4646	34262	4396	33909	33424	3.4	848		

(a) The cross-sections are corrected for double scattering and, being derived from a larger sample, replace those of ref.3.

Table 2: Results of inclusive p_T^2 fits to $Ae^{-Bp_T^2} + Ce^{-Dp_T^2}$ for various reactions. The fits were done for $0.0 \leq p_T^2 \leq 0.7$ $(GeV/c)^2$.

Reaction	p_{in} (GeV/c)	A [mb/(GeV/c)^2]	B [(Gev/c)$^{-2}$]	C [mb/(GeV/c)^2]	D [(GeV/c)$^{-2}$]	χ^2/DOF
$pn \to \pi^- X$	195	881 ± 39	19.5 ± 1.6	263 ± 34	4.6 ± 0.3	16.3/10
$pp \to \pi^- X$	205[a]	304 ± 23	14.6 ± 0.3	80 ± 11	4.0 ± 0.3	6.1/7
$pn \to \pi^- X$	11.6	166 ± 13	11.6 ± 1.1	38 ± 8	4.0 ± 0.3	37.4/16
$pn \to \pi^+ X$	195	889 ± 43	20.2 ± 1.7	257 ± 31	4.3 ± 0.3	19.1/10
$pp \to \pi^+ X$	205[a]	394 ± 20	14.7 ± 0.6	98 ± 3	3.2 ± 0.1	5.6/17
$\pi^+n \to \pi^- X$	195	639 ± 46	20.7 ± 2.6	169 ± 33	4.6 ± 0.5	20.5/10
$\pi^+n \to \pi^+ X$	195	654 ± 36	21.1 ± 2.1	212 ± 25	4.4 ± 0.3	11.2/10

(a) See ref.[8].

Table 3: Average multiplicities for positive $\langle n_+ \rangle$, negative $\langle n_- \rangle$ and charged $\langle n_c \rangle$ particles in the forward and backward c.m. hemispheres for various reactions.

	pp(205 GeV/c) Ref. 8	pn(195 GeV/c) This exp.	π^+n(195 GeV/c) This exp.	π^+p(200 GeV) Ref. 11
$\langle n_- \rangle$				
Backward	1.42 ± 0.02	1.79 ± 0.02	1.67 ± 0.03	
Forward	1.42	1.49 ± 0.02	1.71 ± 0.03	
All	2.84 ± 0.04	3.28 ± 0.03	3.38 ± 0.05	2.95 ± 0.12
$\langle n_+ \rangle$				
Backward	2.42 ± 0.02	1.93 ± 0.02	1.88 ± 0.03	
Forward	2.42	2.35 ± 0.03	2.51 ± 0.05	
All	4.84 ± 0.04	4.28 ± 0.04	4.39 ± 0.05	4.95
$\langle n_c \rangle$				
Backward	3.84 ± 0.04	3.72 ± 0.03	3.55 ± 0.04	
Forward	3.84	3.84 ± 0.03	4.22 ± 0.06	
All	7.68 ± 0.07	7.56 ± 0.06	7.77 ± 0.09	7.90 ± 0.23

Table 4: $\langle p_T \rangle$ values for various reactions

Reaction	p_{in} (GeV/c)	$\langle p_T \rangle$ (Backward) (GeV/c)	$\langle p_T \rangle$ (Forward) (GeV/c)
1. $pn \to \pi^- X$	195	0.336 ± 0.003	0.350 ± 0.005
2. $pn \to \pi^+ X$	195	0.341 ± 0.004	0.361 ± 0.004
3. $\pi^+ n \to \pi^- X$	195	0.336 ± 0.006	0.340 ± 0.006
4. $\pi^+ n \to \pi^+ X$	195	0.327 ± 0.005	0.388 ± 0.006
5. $pn \to p X$ [(a)]	195	(0.454 ± 0.010)	(0.472 ± 0.0013)
6. $\pi^+ n \to p X$ [(a)]	195	(0.478 ± 0.015)	
7. $pp \to \pi^- X$	205	0.336 ± 0.003	
8. $pp \to \pi^+ X$	205	0.373 ± 0.002	
9. $pn \to \pi^- X$	11.6	0.299 ± 0.006	

(a) The p_T values for protons were obtained by using our π^+-p identification procedure and a large systematic error may be anticipated. The errors here, as well as for the other reactions, are statistical only.

Figure Captions

Fig. 1: The inclusive distributions (a) $\frac{d\sigma}{dp_T}$ vs. p_T and (b) $\frac{d\sigma}{dy_{CM}}$ vs. y_{CM} for $pn \to pX$ in the backward c.m. hemisphere. The curves represent Monte-Carlo calculations (see text).

Fig. 2: The inclusive distributions $\frac{d\sigma}{dy_{CM}}$ for (a) $pn \to \pi^{\pm}X$ and (b) $\pi^+n \to \pi^{\pm}X$ at 195 GeV/c.

Fig. 3: The inclusive distributions $\frac{2E}{\pi\sqrt{s}} \cdot \frac{d\sigma}{dx}$ for (a) $pn \to \pi^{\pm}X$ and (b) $\pi^+n \to \pi^{\pm}X$ at 195 GeV/c.

Fig. 4: The inclusive distribution $\frac{d\sigma}{dy_{LAB}}$ for π^- in $pn \to \pi^-X$ at 11.6 and 195 GeV/c.

Fig. 5: The inclusive distributions $\frac{1}{\sigma_{inel}} \cdot \frac{d\sigma}{dy_{CM}}$ for (a) π^- and (b) π^+ in $pn \to \pi^{\pm}X$ and $\pi^+n \to \pi^{\pm}X$ at 195 GeV/c.

Fig. 6: The inclusive distribution $\frac{d\sigma}{dy_{CM}}$ for π^- in $pn \to \pi^-X$ compared to $\frac{d\sigma}{dy_{CM}}$ for π^- in $pp \to \pi^-X$ (ref. [8]).

Fig. 7: (a) The inclusive distribution $\frac{d\sigma}{dp_{\pi^-}^2}$ for π^- in the reactions: $pn \to \pi^-X$ (195 GeV/c), $pn \to \pi^-X$ (11.6 GeV/c), $pp \to \pi^-X$ (205 GeV/c, ref. [8]) and $\pi^+n \to \pi^-X$ (195 GeV/c). (b) The inclusive distribution $\frac{d\sigma}{dp_T^2}$ for π^+ in the reactions: $pn \to \pi^+X$ and $\pi^+n \to \pi^+X$ at 195 GeV/c.

Fig. 8: The inclusive distribution $\frac{d\sigma}{dy_{CM}}$ for pions in the reactions: (a) $pn \to \pi^-X$, (b) $pn \to \pi^+X$, (c) $\pi^+n \to \pi^-X$ and (d) $\pi^+n \to \pi^+X$ at 195 GeV/c. The distributions are shown for three multiplicity groups: 3-5 prongs (circles), 7-9 prongs (triangles) and for more than 9 prongs (crosses).

Fig. 9: The ratio R' between positive and negative pions as a function of the c.m. rapidity y_{CM} in $pn \to \pi^{\pm}X$ (circles) and in $\pi^+n \to \pi^{\pm}X$ (triangles) at 195 GeV/c. R' is defined as π^+/π^- for $y_{CM} > 0.0$ and as π^-/π^+ for $y_{CM} < 0.0$ (see text).

Fig. 10: Circles represent $\delta_1 = \frac{d\sigma(pn \to \pi^-X)}{dy}(y) - \frac{d\sigma(pp \to \pi^-X)}{dy}(y)$ evaluated for $y<0$. (backward c.m. hemisphere). Triangles represent $\delta_2 = \frac{d\sigma(y)}{dy} - \frac{d\sigma(-y)}{dy}$ (i.e. the backward minus forward cross-sections for $pn \to \pi^-X$). δ_1 and δ_2 measure the excess of π^-'s in the neutron hemisphere over the proton hemisphere.

Fig. 11: "Normalized" inclusive π^- distributions for $pp \to \pi^-X$ (circles, at 205 GeV/c) and $pn \to \pi^-X$ (triangles, at 195 GeV/c). The pp distributions are from ref. [8]. The comparison is done for three multiplicity groups: (a) 3-5 prongs, (b) 7-9 prongs and (c) more than 9 prongs.

Fig. 12: Ratio of the number of prongs (negative or positive) emitted in the backward c.m. hemisphere (N_B) to the total number of prongs (N_T) for the reactions: (a) pn and (b) π^+n at 195 GeV/c. Circles denote negative prongs and triangles positive prongs.

Fig. 13: Average transverse momenta, $\langle p_T \rangle$, of π^+'s (open circles) and π^-'s (full circles) in the reactions $pn \to \pi^{\pm}X$ and $\pi^+n \to \pi^{\pm}X$ at 195 GeV/c as a function of x in (a), (b) and as a function of x_R in (c), (d).

Fig. 14: Average transverse momenta, $\langle p_T \rangle$ of π^+'s (open circles) and π^-'s (full circles) in the reactions $pn \to \pi^{\pm}X$ and $\pi^+n \to \pi^{\pm}X$ at 195 GeV/c. $\langle p_T \rangle$ is plotted vs. rapidity (y_{CM}) in (a), (b) and vs. multiplicity (n) in (c), (d).

Fig. 15: Average transverse momenta, $\langle p_T \rangle$, of pions in backward ($\langle p_T^{\pm} \rangle_B$) and forward ($\langle p_T^{\pm} \rangle_F$) c.m. hemispheres for the reactions $pn \to \pi^{\pm} X$ and $\pi^+ n \to \pi^{\pm} X$ at 195 GeV/c.

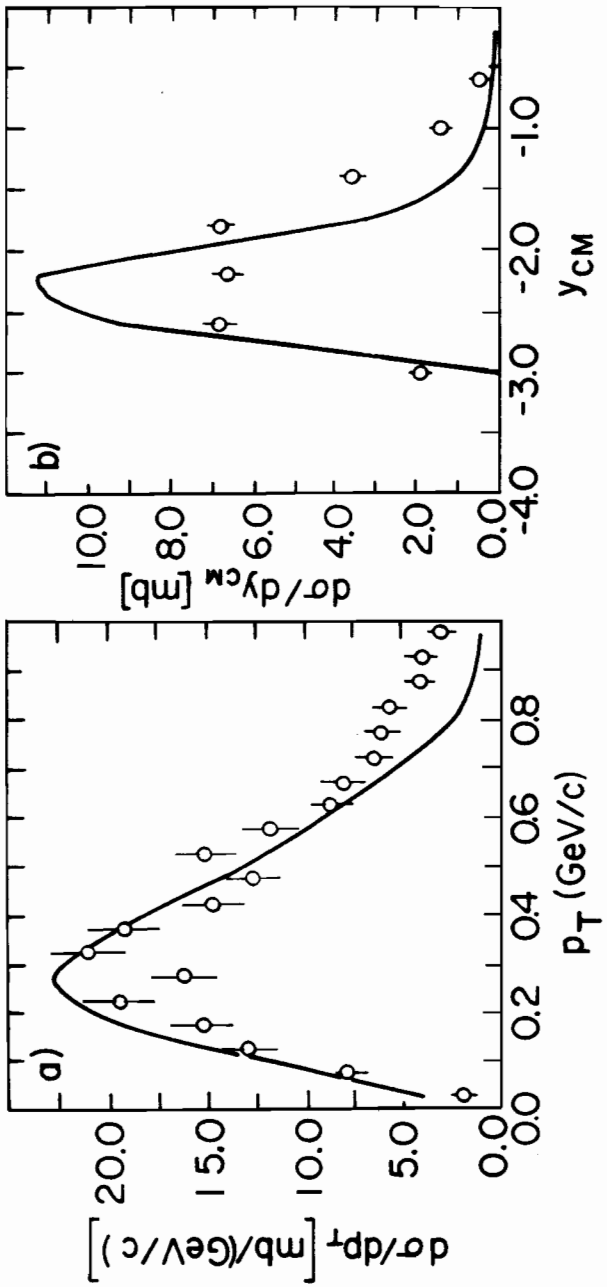

Fig. 1

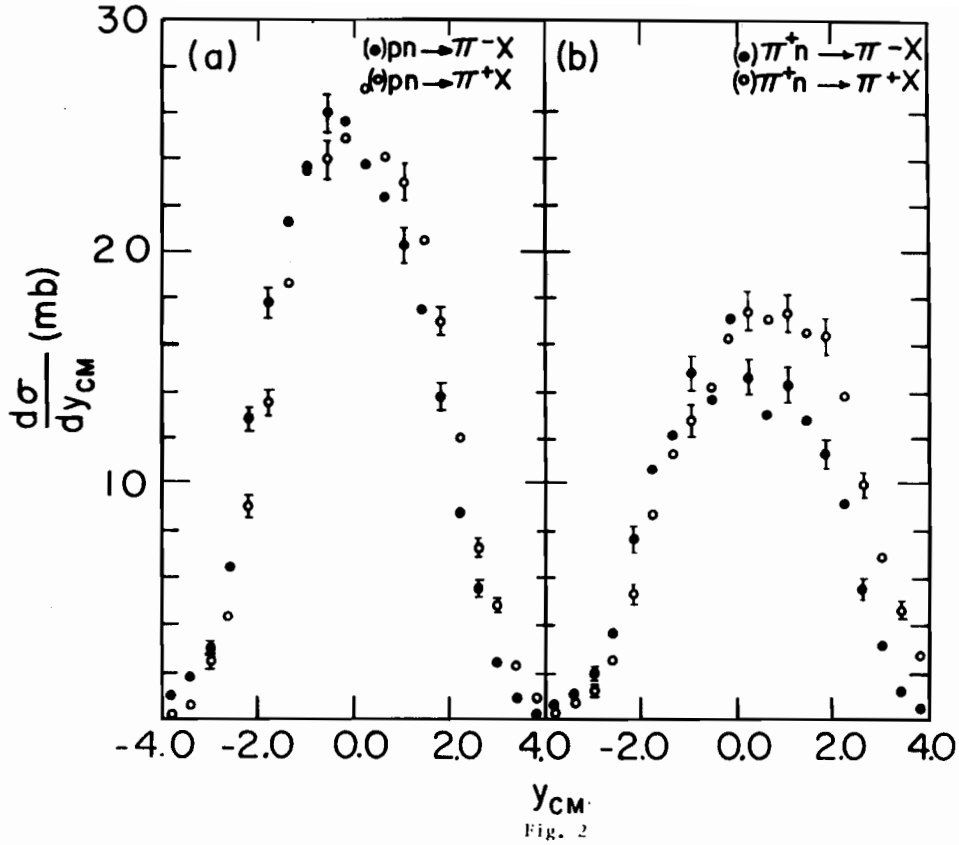
(a)
(•)pn→π⁻X
(◦)pn→π⁺X
(b)
(•)π⁺n→π⁻X
(◦)π⁺n→π⁺X
dσ/dy_CM (mb)
y_CM

Fig. 2

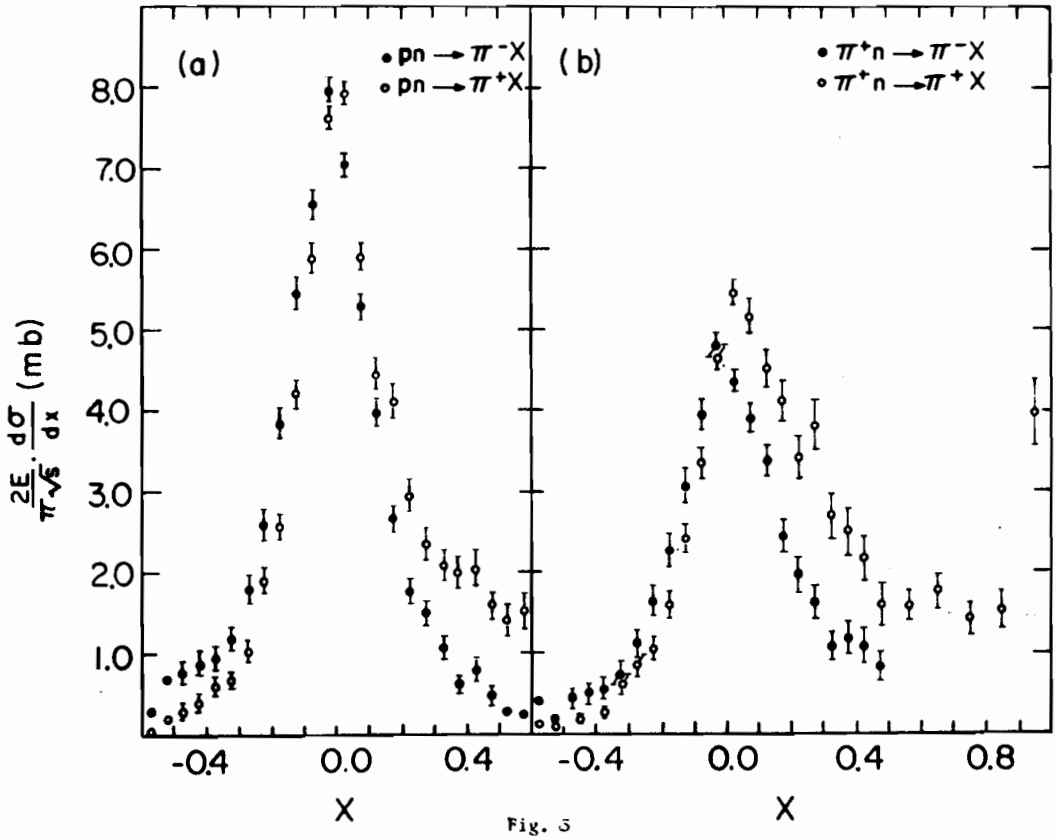
(a)
• pn→π⁻X
◦ pn→π⁺X
(b)
• π⁺n→π⁻X
◦ π⁺n→π⁺X
2E/π√s · dσ/dx (mb)
X

Fig. 3

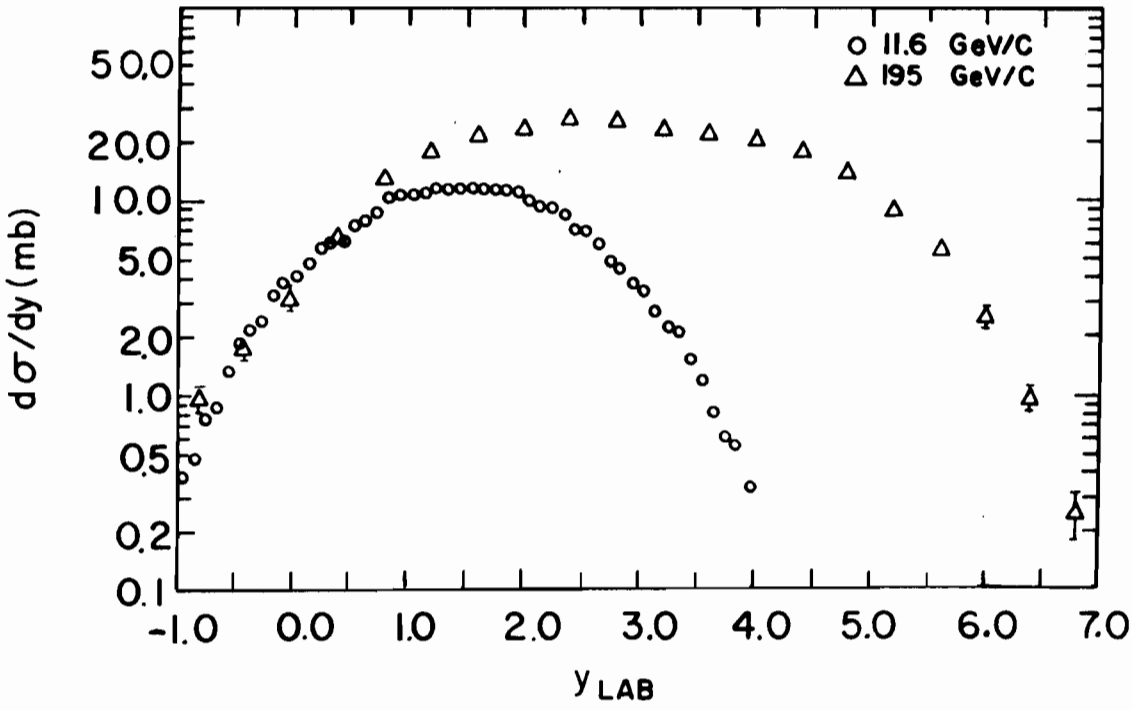
o 11.6 GeV/C
Δ 195 GeV/C
50.0
20.0
10.0
5.0
2.0
1.0
0.5
0.2
0.1
dσ/dy (mb)
-1.0
0.0
1.0
2.0
3.0
4.0
5.0
6.0
7.0
y LAB

Fig. 4

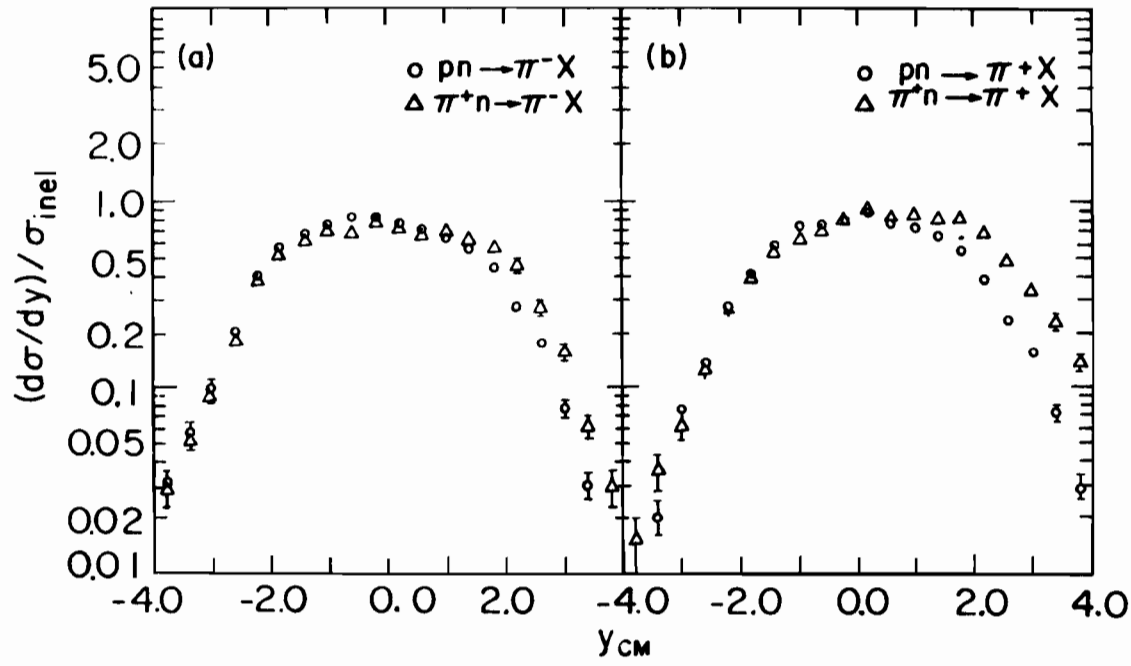
(a)
o pn → π⁻X
Δ π⁺n → π⁻X
(b)
o pn → π⁺X
Δ π⁺n → π⁺X
5.0
2.0
1.0
0.5
0.2
0.1
0.05
0.02
0.01
(dσ/dy)/σinel
-4.0
-2.0
0.0
2.0
-4.0
-2.0
0.0
2.0
4.0
yCM

Fig. 5

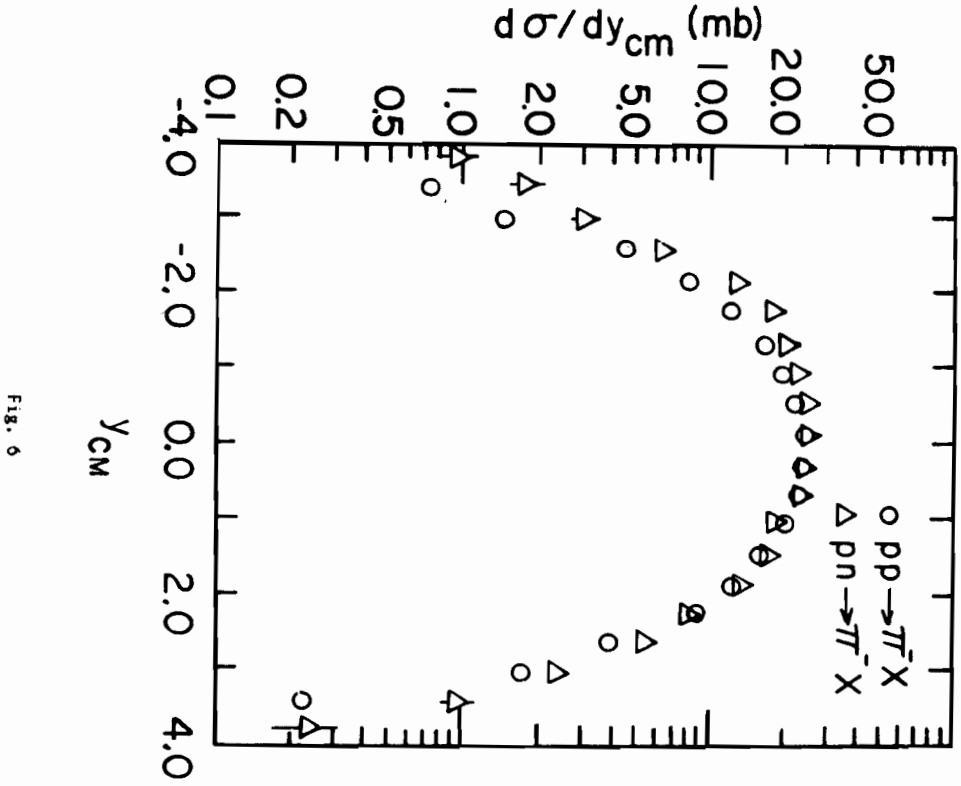
dσ/dy_cm (mb)
0.1
0.2
0.5
1.0
2.0
5.0
10.0
20.0
50.0
-4.0
-2.0
0.0
2.0
4.0
y_CM
o pp→π⁻X
Δ pn→π⁻X

Fig. 6

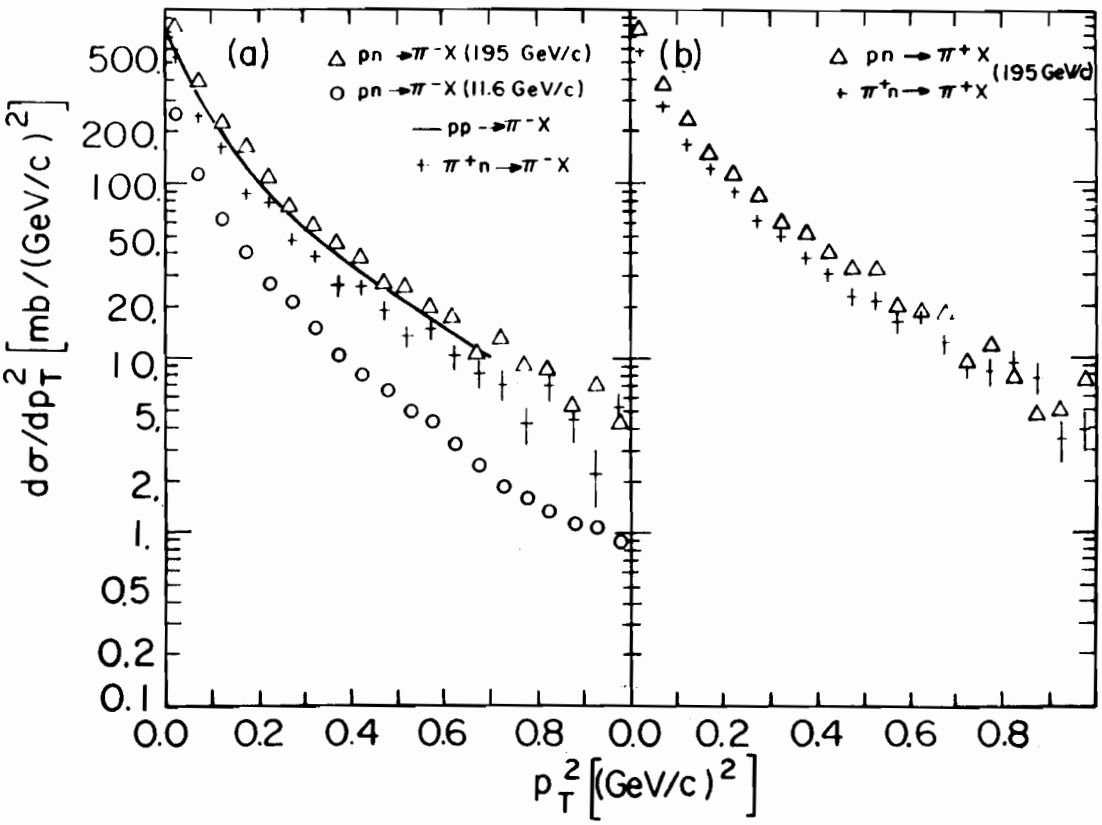
(a)
Δ pn →π⁻X (195 GeV/c)
o pn →π⁻X (11.6 GeV/c)
— pp →π⁻X
+ π⁺n →π⁻X
(b)
Δ pn → π⁺X (195 GeV/c)
+ π⁺n → π⁺X
dσ/dp_T² [mb/(GeV/c)²]
500.
200.
100.
50.
20.
10.
5.
2.
1.
0.5
0.2
0.1
0.0
0.2
0.4
0.6
0.8
p_T² [(GeV/c)²]

Fig. 7

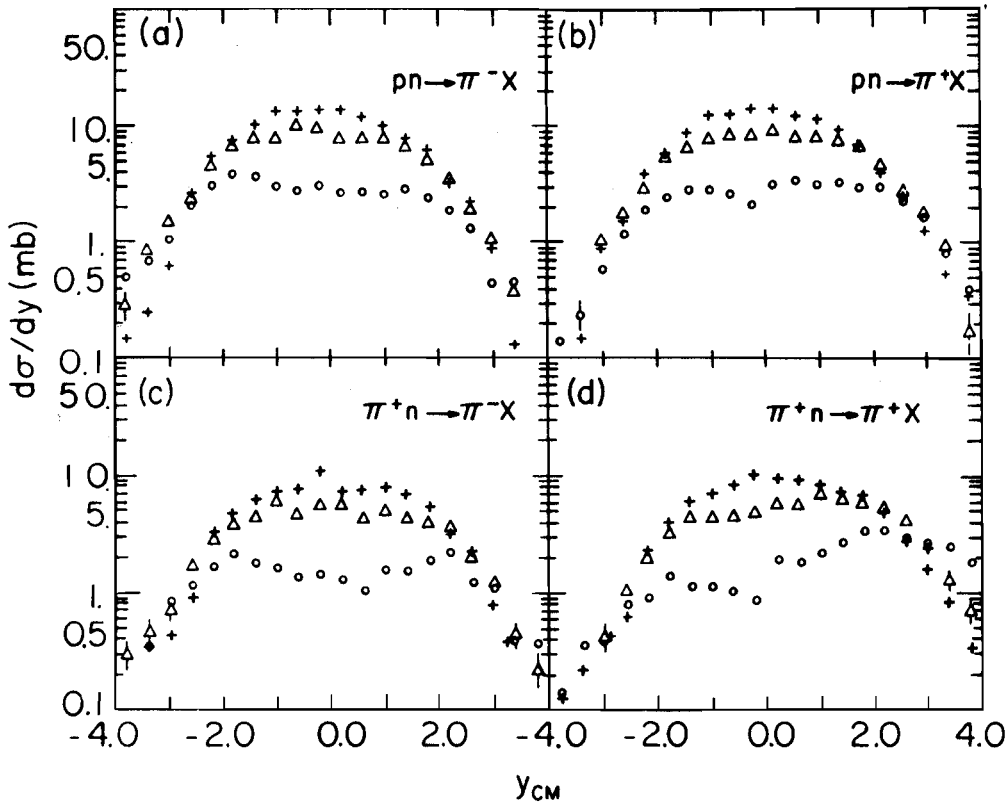
(a)
pn→π⁻X
(b)
pn→π⁺X
(c)
π⁺n→π⁻X
(d)
π⁺n→π⁺X
dσ/dy (mb)
50.
10.
5.
1.
0.5
0.1
-4.0
-2.0
0.0
2.0
4.0
y_CM

Fig. 8

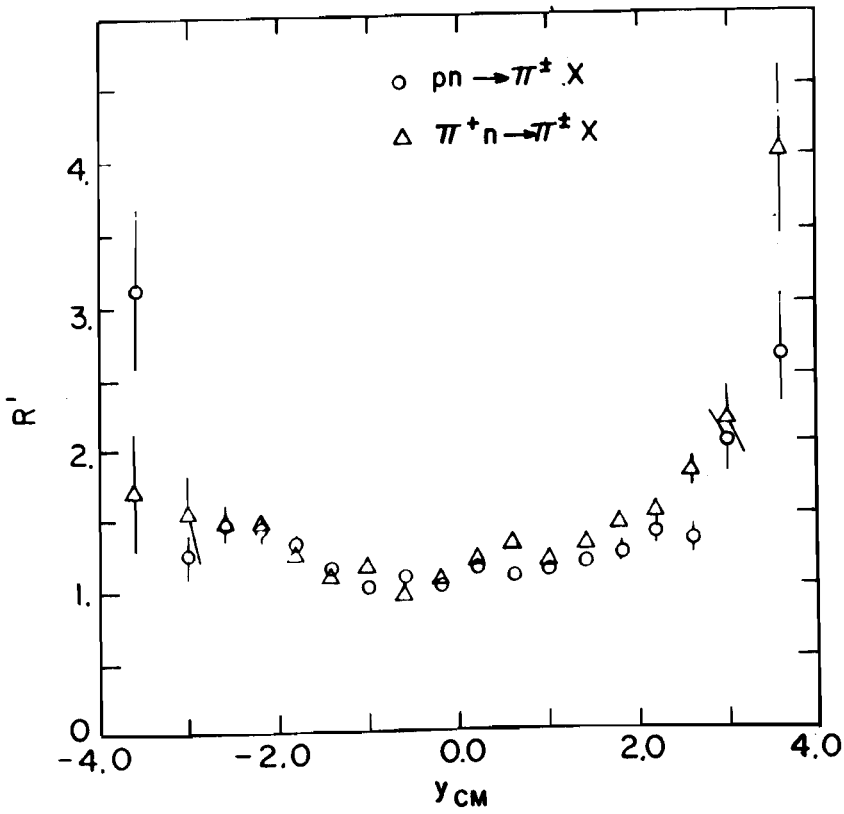
pn→π±X
π⁺n→π±X
R⁻
4.
3.
2.
1.
0
-4.0
-2.0
0.0
2.0
4.0
y_CM

Fig. 9

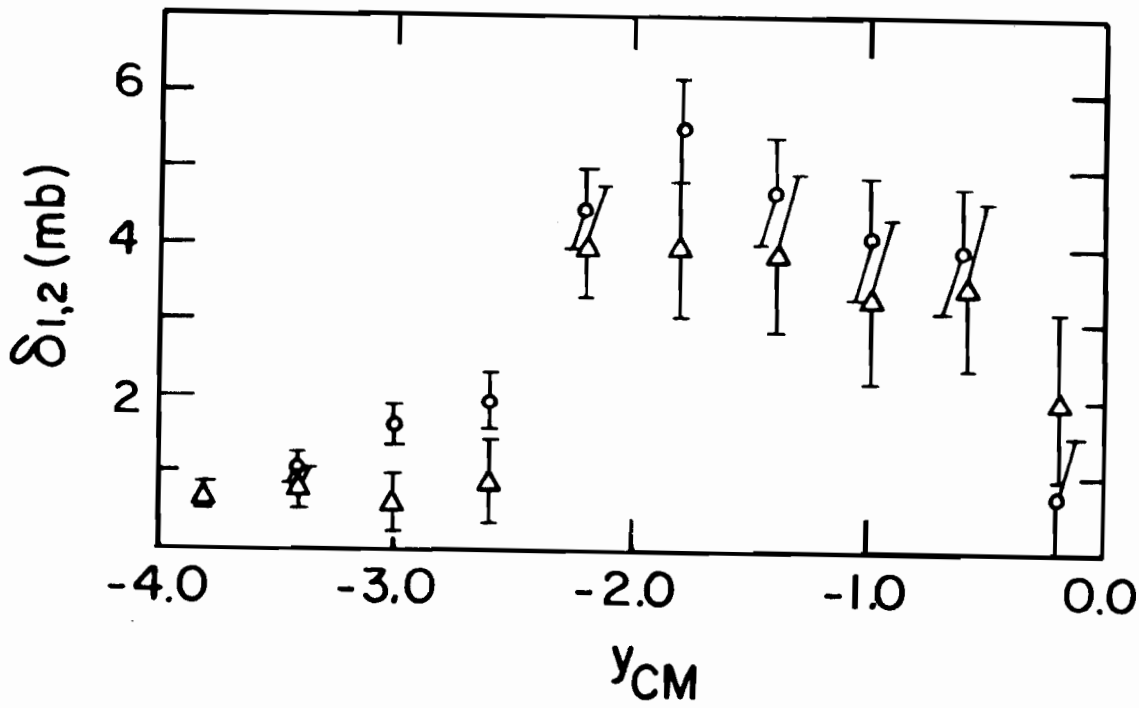
6
4
2
$\delta_{1,2}$ (mb)
-4.0
-3.0
-2.0
-1.0
0.0
y_{CM}

Fig. 10

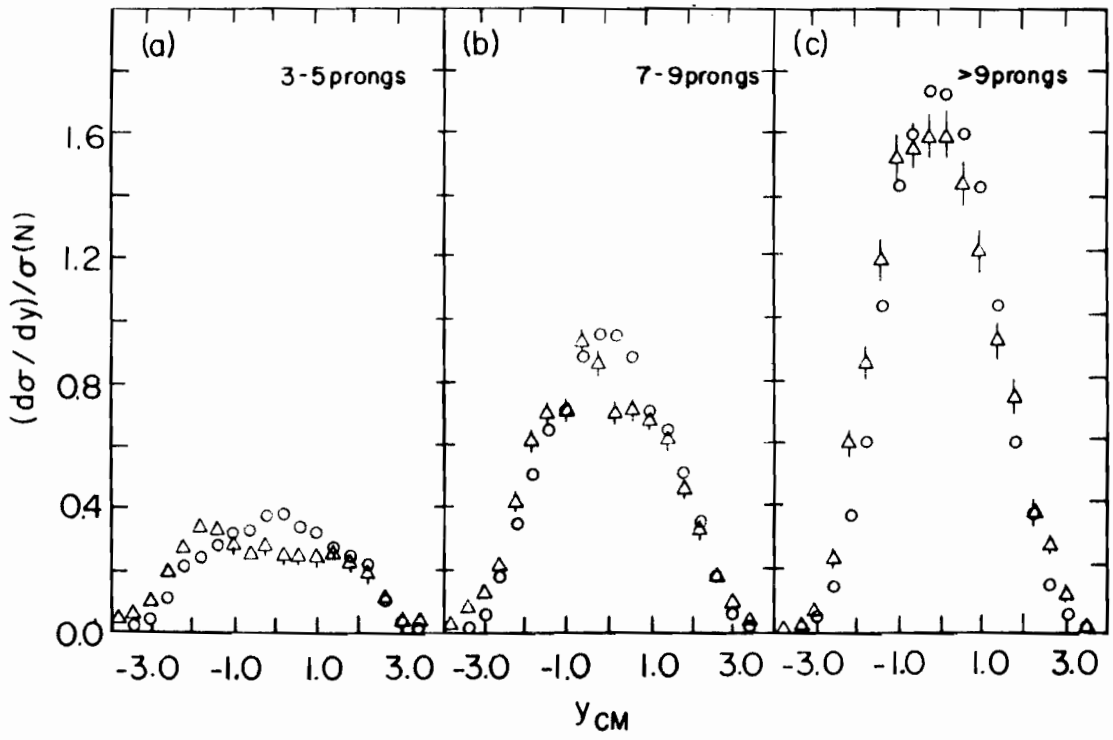
(a)
3-5prongs
(b)
7-9prongs
(c)
>9prongs
1.6
1.2
0.8
0.4
0.0
$(d\sigma/dy)/\sigma(N)$
-3.0
-1.0
1.0
3.0
y_{CM}

Fig. 11

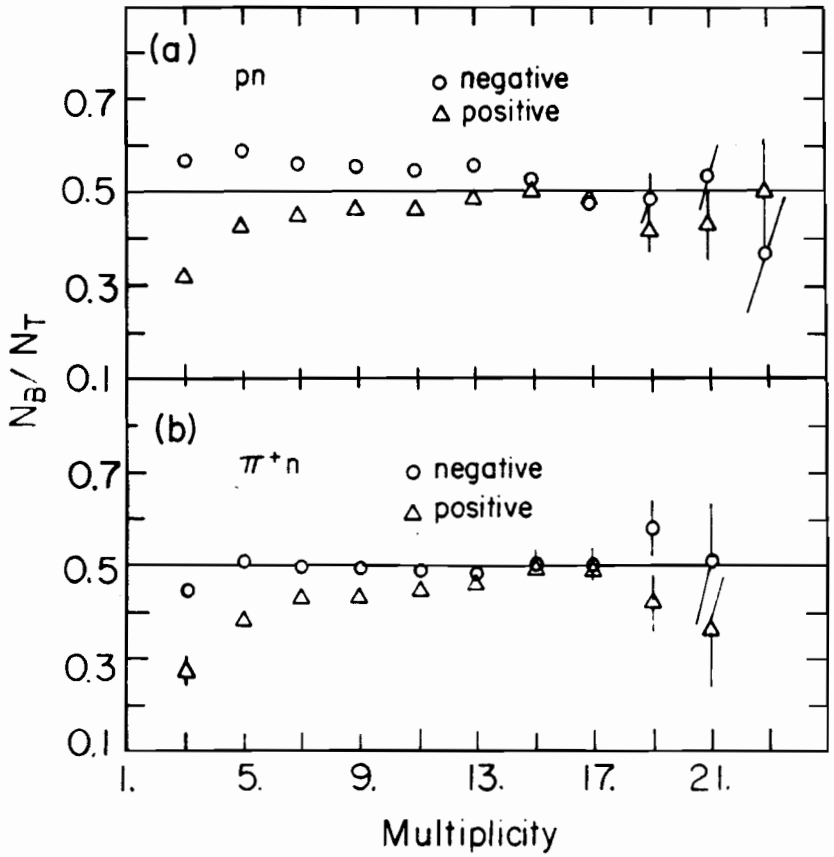
(a)
pn
o negative
Δ positive
(b)
π⁺n
o negative
Δ positive
N_B / N_T
0.7
0.5
0.3
0.1
1.
5.
9.
13.
17.
21.
Multiplicity

Fig. 12

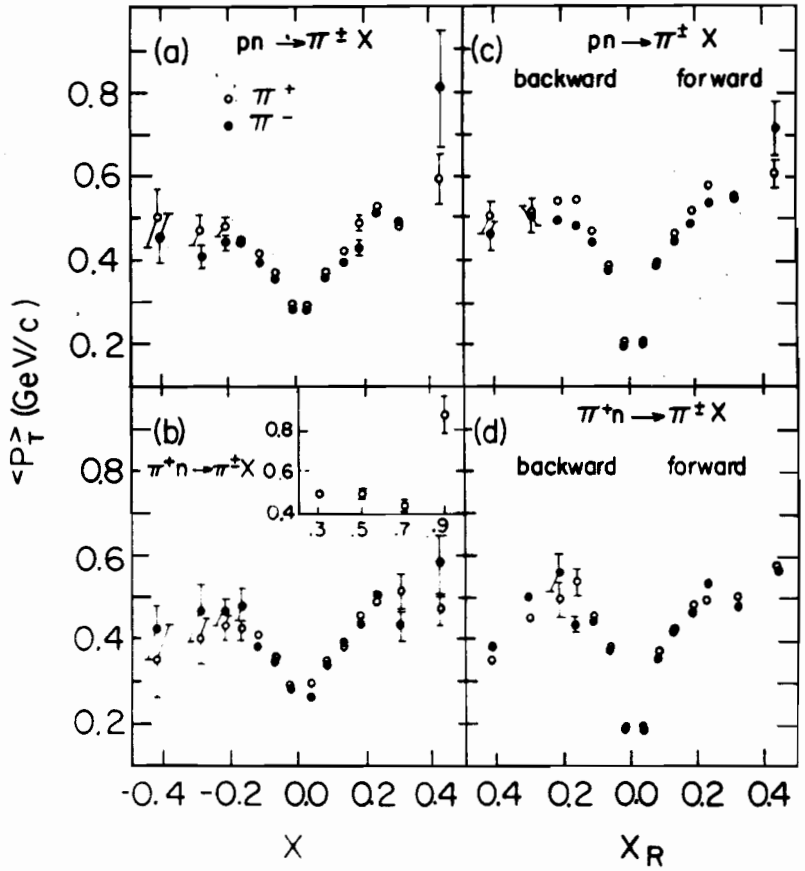
(a) pn → π± X
π⁺
π⁻
(c) pn → π± X
backward
forward
(b) π⁺n → π± X
(d) π⁺n → π± X
backward
forward
<P_T> (GeV/c)
0.8
0.6
0.4
0.2
-0.4 -0.2 0.0 0.2 0.4
0.4 0.2 0.0 0.2 0.4
X
X_R

Fig. 13

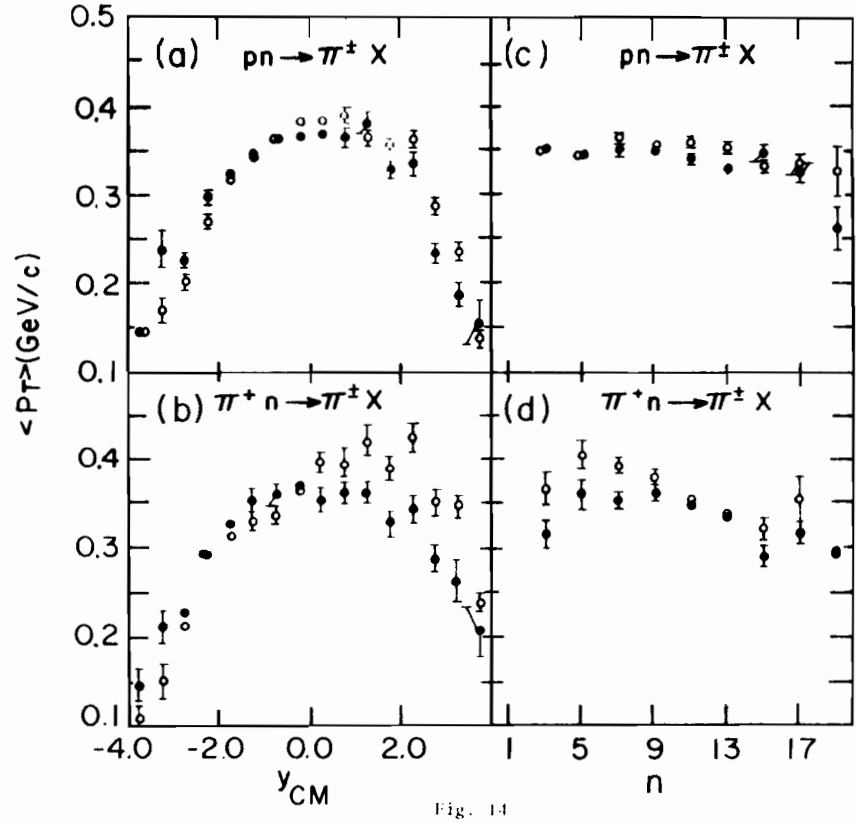
(a) pn → π± X
(c) pn → π± X
(b) π⁺n → π± X
(d) π⁺n → π± X
<PT>(GeV/c)
0.5
0.4
0.3
0.2
0.1
-4.0
-2.0
0.0
2.0
yCM
1
5
9
13
17
n

Fig. 14

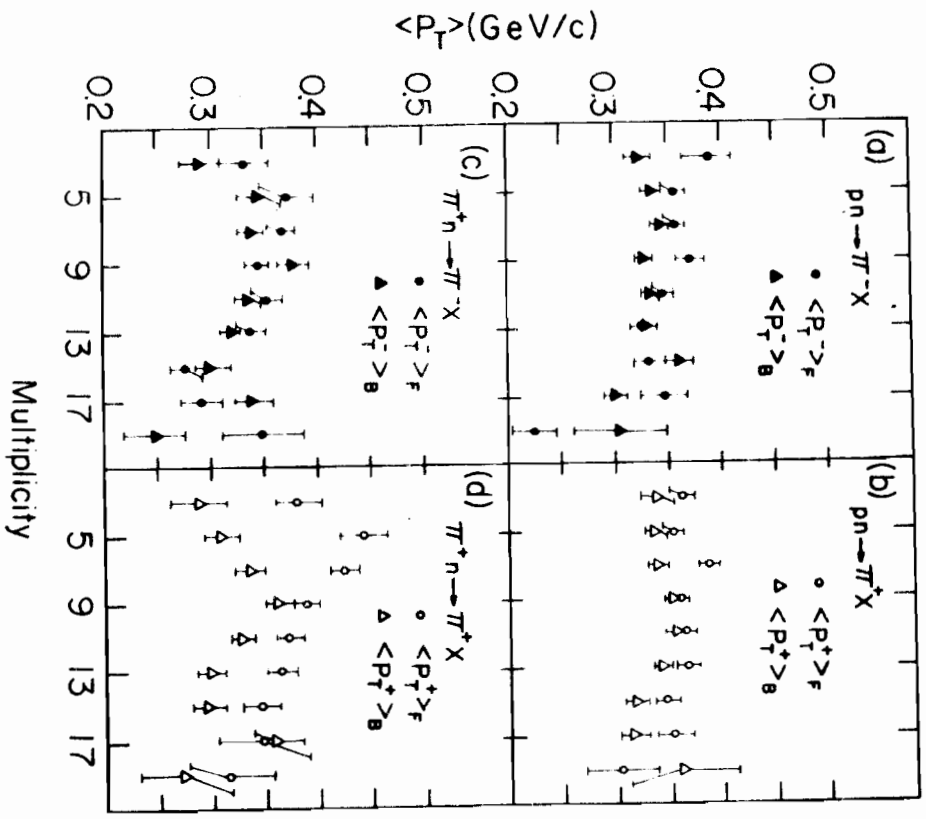
<PT>(GeV/c)
0.2
0.3
0.4
0.5
Multiplicity
5
9
13
17
(a) pn → π⁻X
• <PT⁻>F
▲ <PT⁻>B
(b) pn → π⁺X
• <PT⁺>F
▲ <PT⁺>B
(c) π⁺n → π⁻X
• <PT⁻>F
▲ <PT⁻>B
(d) π⁺n → π⁺X
• <PT⁺>F
▲ <PT⁺>B

Fig. 15